Advances in Natural and Applied Sciences, 9(12) August 2015, Pages: 71-80

AENSI Journals

Advances in Natural and Applied Sciences

ISSN:1995-0772 EISSN: 1998-1090
Journal home page: www.aensiweb.com/ANAS

Facial Forehead Wrinkles Detection using Colour based Skin Segmentation

[1]Arumugam P, [2]Selvakumar S and [3]Muthukumar Subramanyam

[1]*Department of Statistics, MS University, Tirunelveli-627012, Tamil Nadu.*
[2]*Research Scholar, MS University, Tirunelveli-627012, Tamil Nadu.*
[3]*Professor, Dhirajlal Gandhi College of Technology, Dept. of computer science and engineering, Salem, Tamil Nadu.*

ARTICLE INFO

Article history:
Received 23 July 2015
Accepted 28 August 2015
Available online 25 September 2015

Keywords:
Skin Segmentation, Face detection, Wrinkle, forehead, Image processing, color space

ABSTRACT

Facial wrinkles are an undesirable feature caused by extrinsic photo damage and intrinsic aging process. Many cosmetic products and esthetical procedures strive to ameliorate the appearance of wrinkles. Currently the effects of those products and procedures on wrinkles are mainly evaluated by clinical grading, subjective self-assessment questionnaires, and optical profilometry of replica impressions. An objective and quantitative method is in demand. The onus is on all serious physicians to objectively evaluate these products before they become extensively implemented.
This is the first work involving age classification, and the first work that successfully extracts and uses natural wrinkles. It is also a successful demonstration that facial features are sufficient for a classification task, a finding that is important to the debate about what are appropriate representations for facial analysis. Nowadays, documenting the face appearance through imaging is prevalent in skin research, therefore detection and quantitative assessment of the degree of facial wrinkling is a useful tool for establishing an objective baseline and for communicating benefits to facial appearance due to cosmetic procedures or product applications. In this work, an algorithm for automatic detection of facial wrinkles is developed, based on estimating the orientation and the frequency of elongated features apparent on faces. By over-filtering the skin texture image with finely tuned oriented Gabor filters, an enhanced skin image is created. The wrinkles are detected by adaptively thresholding the enhanced image, and the degree of wrinkling is estimated based on the magnitude of the filter responses.

To Cite This Article: Arumugam P, Selvakumar S and Muthukumar Subramanyam, Facial Forehead Wrinkles Detection using Colour based Skin Segmentation. **Adv. in Nat. Appl. Sci.,** *9(12): 71-80, 2015*

INTRODUCTION

The Ageing effect in human mostly revealed in head and face. This research is spanning to the topics related to anthropology and biology, medicine and pathology, and computer and forensic science. Human face is a prolific information source, where people can effortlessly extract many kinds of useful information from a face image, such as identity, expression, emotion, gaze, gender, age, *etc*. skin undergoes both intrinsic and extrinsic aging processes. Like all the other organs in the body, the skin progressively decreases in its functional capacity as our age increases. Also, it is a well-known fact that the biodynamic factors of facial aging are quite different for the two stages of aging: growth and development and adult. During the latter, the major changes in facial complex are due to lengthening and widening factors of cranial complex. The most significant aging factor for adults includes some cranial changes, but the primary drivers are the development of wrinkles, lines, creases, and sagging of the skin. Chronic sun exposure especially to the UV wavelength accelerates damage to the epidermis and the dermis, that resulting in the appearance of wrinkles, mottled pigmentation, and skin sagging (Tieu, 2002; Hamilton, 1998). There is a great consumer demand for products and procedures that improve the appearance of aging skin by helping the skin to maintain a more radiant and youthful look. Many researchers have been conducted to understand the mechanism of skin aging and photodamage (Tieu, 2002; Hamilton, 1998; Stegman, 1987). Many research trials are conducted each year on medical devices, prescription products, and cosmetic products to evaluate their effectiveness in improving the texture, color, and contour features of aging skin.

The aim of this research is to integrate key findings from this broad review literature to understand that patterns, rates, and characteristics of aging may be different due to culture and lifestyle (environment, gender) and biology (sex, ancestry or genetics, trauma and disease), as well as idiosyncratic features, such as frequency and extent of facial expressions. The way in which patterns, rates and or characteristics of aging vary among

Corresponding Author: Arumugam, P, Department of Statistics, MS University, Tirunelveli-627012, Tamil Nadu.

people at any given age, or change over time in any one person, are not completely understood. The specific challenges with age classification are that the age of the person is hard to predict exactly because facial appearance changes slowly when a person is aging and this change in appearance is somewhat person dependent.

The clear distinction among wrinkles, furrows, and folds is difficult because there is no commonly accepted classification or body of terminology that is based on anatomic, dimensional, or etiologic criteria. Words such as wrinkles, lines, furrows, and folds are used with heavy reliance on the intuitive grasp. Superficial wrinkles are associated with textural changes of the skin surface caused by intrinsic aging and photoaging of topographically defined areas. The fine lines of wrinkling may be discrete at first and then, over time, become grouped and multidirectional as noted by Stegman. (Hamilton, 1998). Wrinkle lines are usually limited to superficial dermal creasing; thus, they are amenable to treatments such as chemical peeling, dermabrasion, and laser resurfacing.) Stegman, S.J., 1987 ; Lask, 1995; Grover, 1998; Fitzpatrick, 1996) Mimetic wrinkles, commonly referred to as lines (partial thickness) or furrows (full thickness), are the visible effects of deep dermal creasing caused by repeated facial movement and expression combined with dermal elastosis. They are therefore perpendicular to the direction of the underlying facial muscles. They occur with aging as forehead and glabellar lines, nasolabial folds, radial lip lines, marionette lines, and lines in the corners of the mouth. Folds are the result of overlapping skin caused by genetic laxity, intrinsic aging, loss of tone, bony atrophy, gravity, and consequent sagging. They occur as upper and lower lid folds in blepharoptosis, as nasolabial folds in midface sagging, and as horizontal neck folds in lax skin. The correction of folds requires tightening procedures such as blepharoplasty, face lift, or direct skin excision. (Kligman, 19985) Augmentation of the bony skeleton by implants, bone grafts, or skeletal osteotomies may also be necessary to treat folds in properly selected cases. Combinations of mimetic wrinkles and folds are commonly present. A sagging fold may be temporarily eliminated by manual elevation, exposing a crease or furrow in its center.

Classifications of facial wrinkles:

The challenges associated with face and facial feature detection can be attributed to the following factors (Nallaperumal, 2013).

• Intensity. There are three types of intensity: color, gray, and binary.

• Pose. Face images vary due to the relative camera-face pose (frontal, 45_, profile), and some facial features such as an eye may become partially or wholly occluded.

• Structural components. Facial features such as beards, mustaches, and glasses may or may not be presented.

• Image rotation. Face images directly vary for different rotations.

• Poor quality. Image intensity in poor-quality images, for instance, blurry images, distorted images, and images with noise, becomes unusual.

• Facial expression. The appearance of faces depends on a personal facial expression.

• Unnatural intensity. Cartoon faces and rendered faces from 3D model have unnatural intensity.

• Occlusion. Faces may be partially occluded by other objects such as hand, scarf, etc.

• Illumination. Face images vary due to the position of light source.

In recent surveys, there are five categories of face and facial feature detection.

(1) Geometry-based methods. These methods utilize geometrical information (Tieu, 2002; Stegman, S.J., 1987). Each feature is demonstrated as a geometrical shape. They can accurately detect face and facial features, but cannot handle large variations of the face images such as images with some occluded facial features and images with noise.

(2) Color-based approaches. These approaches face difficulties in robustly detecting skin colors in the presence of complex background and different illuminations (Lask, 1995; Grover, 1998; Fitzpatrick, 1996; Glogau, R.G., 1996). These algorithms are applicable only for color images.

(3) Appearance-based methods. These methods use the models learned from a set of training images (Olenius, M., 1998; Marks, R., 1990; Grove, 1989; Gormley, 1988; Rohr, 1998). Gray value (intensity) is the most important parameter for the detection. They are not able to perfectly detect face images with poor quality in intensity, some occlusions, and unnatural intensity.

(4) Motion-based methods. Face and facial features are detected from the image sequence (Kligman, 1985; Tan, 1982; Eisenbeiss, 2001). Using such methods, facial features cannot be detected using only a single still image from one view.

(5) Edge-based methods. In the last class of methods (Muthukumar Subramanyam, 2014; Chang, Chuan-Yu, 2010; Muthukumar Subramanyam, 2015), faces are detected without information due to intensity and motion. The edge information is used as input. These methods can handle large variations of the face images. However, these methods detect only face or facial features(Muthukumar Subramanyam, 2014; Chang, Chuan-Yu, 2010; Muthukumar Subramanyam, 2015).

Fitzpatrick (1996) proposed a classification of perioral and periorbital wrinkling for use in establishing the effect of laser resurfacing of the skin (Table I). Fitzpatrick's classification was directed toward generalized wrinkling and elastosis rather than specific wrinkle depth. Wrinkle depth analysis,

which is not accounted for by the Fitzpatrick (1996) scale, is a more important measurement when considering wrinkle augmentation with injectable fillers. Glogau8 has proposed a classification consisting of type I (no wrinkles), type II (wrinkles in motion), type III (wrinkles at rest), and type IV (only wrinkles). These classifications are confined to generalized wrinkles and do not address specific mimetic wrinkles or folds Fitzpatrick (1996).

Table 1: Fitzpatrick's Classification of Facial Wrinkling

Wrinkling	Score	Class
Fine wrinkles	1–3	I
Fine to moderate depth wrinkles, moderate number of lines	4–6	II
Fine to deep wrinkles, Numerous lines, with or without redundant skin	7–9	III

The only classification to include facial wrinkles, furrows, and folds was published by Hamilton. 15 A choice of appropriate therapy results simply from categorizing the patient's problems with this comprehensive and easily understandable chart (Table II). However, this classification, oriented toward treatment selection, provides no scale to objectively measure the outcome of treatment.

Facial wrikles anatomy & measurements:

The first attempts to use quantitative methods have been described only recently4–6 and developed for the assessment of facial skin rejuvenation after laser treatment of wrinkles. Facial wrinkles were measured directly by use of a simple light microscope, a technique confirmed by electron microscopy. A review of the literature [3, 7, 8, 15] and current practice revealed that there is not an appropriate classification system for deep facial wrinkles and folds. Objective measurements, however, are necessary to rate the effect of treatments with injectable materials. In daily practice, a simple look at a reliable reference scale would enable clinicians to classify the deep mimetic wrinkles and folds on a patient's face. To develop a scale for the assessment of skin fillers used in the treatment of facial mimetic wrinkles or furrows. The goal is to determine whether a photographically based classification of mimetic wrinkles could be used reliably and consistently by clinicians and to determine whether this classification correlated with measurement of wrinkle depth as determined by profilometry on negative silicone replicas of facial wrinkles.

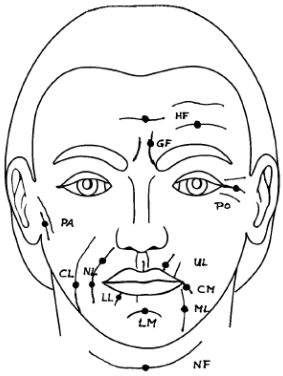

Fig. 2: Anatomic reference points for assessment and measurement of wrinkle depth.

If the deepest point of the wrinkle is outside of this point, it can be marked or described separately. HF, horizontal forehead lines; GF, glabellar frown lines; PO, periorbital lines; PA, preauricular lines; CL, cheek lines; NL, nasolabial folds; UL, upper radial lip lines; LL, lower radial lip lines; CM, corner of the mouth lines; ML, marionette lines;LM, labiomental crease; NF, horizontal neck folds.

Table 2: Hamilton's Classification of Contour Changes of Facial Skin.

Facial Aging	Clinical Morphology	Tissue Location	Clinical Location	Etiology
A	Folds	Muscular	Nasolabial folds, neck, eyelids	Loss of tone, gravity
B	Furrows	Musculocutaneous	Forehead, smile lines	Repeated facial expressions
C	Wrinkles	Cutaneous	Cheeks, crow's feet, perioral	Intrinsic aging, photoaging
D	Combination			

Horizontal Forehead Lines:

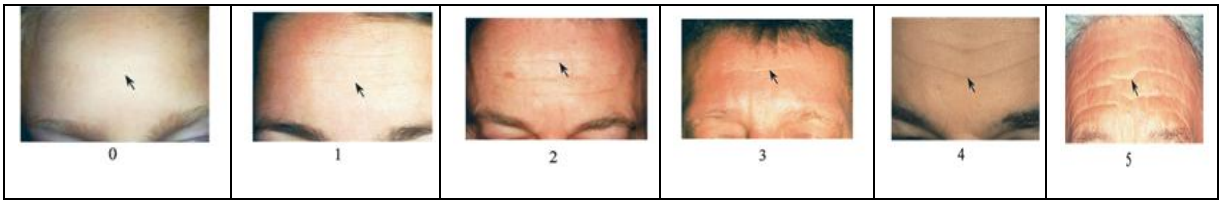

Fig. 3: Wrinkle Assessment Scale of horizontal forehead lines.

Table 3: Classification of Facial Wrinkles

Facial Wrinkle	Class	Description
Horizontal forehead lines Glabellar frown lines	0	No wrinkles
	1	Just perceptible wrinkle
	2	Shallow wrinkles
	3	Moderately deep wrinkle
	4	Deep wrinkle, well-defined edges
	5	Very deep wrinkle, redundant fold

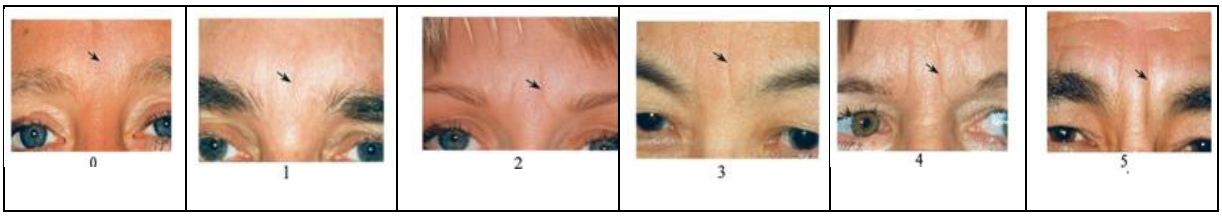

Fig. 4: Wrinkle Assessment Scale of glabellar frown lines.

Table 4: Popular Color Spaces used for Skin Segmentation

SrNo	Colour Space Group	Colour Space Examples
1	RGB	RGB, Normalized RGB, XYZ, CIE
2	Perceptual Colour Spaces	HIS, HSV, HSL, TSL, TSV
3	Orthognal Colour Spaces	YCbCr, YIQ, YES , YUV
4	Perceptually Uniform Colours	CIELAB, CIELUV,CIE XYZ, CIE-xyY

Wrinkle Assessment Scale From hundreds of pictures taken from randomized patients in the first author's practice (G. Lemperle), one reference photograph was selected for each class (0 to 5) of facial wrinkles from 11 different regions (Fig. 2). As a result, reference picture sheets were created (Figs. 3 through 13) for use in validating the reliability of photographic classification. The photographs of the Wrinkle Assessment Scale were used "live" in direct comparison with the corresponding wrinkle or fold in the patient's face or "indirectly" by comparing a patient's photograph with the pictures of the scale. The assessment was always made at the same location by use of anatomic landmarks(Fig. 2). Horizontal forehead lines were measured at their intersection with the vertical pupillary line. Glabellar frown lines were measured at the level of the upper border of the eyebrows.

Colour-based skin segmentation:

As the human skin seems to have a characteristic range of colour, many skin detection approaches are based on classifying pixels using their colour (Forsyth and Ponce, 2003). A wide set of colour spaces have been considered to model the skin chrominance (Vezhnevets *et al*., 2003)(Kakumanu *et al*., 2007). However, according to (Albiol *et al*.,): "for all colour spaces their corresponding optimum skin detectors have the same performance since the separability in skin or not skin classes is independent of the colour space chosen". In other words, the quality of a skin detection method is more dependent on the proposed detection algorithm and less on the used colour space. In this section, in order to investigate this statement, three colour spaces are used to represent the human skin: RGB, HSV and YCbCr. For the case of basic RGB space, we applied the following simple explicit skin detection algorithm that can be found in (Kovac *et al*., 2003) and works on all the image pixels for uniform daylight illumination:

$$(R > 95) \wedge (G > 40) \wedge (B > 20) \wedge (maxR, G, B - minR, G, B > 15) \wedge (|R - G| > 15) \wedge (R > G) \wedge (R > B) \quad (1)$$

where R, G and B represent the value of pixel in the respective RGB colour channel with values ranging from 0 to 255. For HSV and YCbCr spaces, a similar approach is followed. We retain luminance information by converting the image to gray levels. Next, we produce an initial over segmented image of regions by applying a morphological watershed method. For each produced watershed region their corresponding colour histograms for each of the three channels (in HSV or YCbCr spaces) are computed and compared using the Battachariyya distance (Kailath, 1967) to the corresponding previous trained skin histograms. If these histograms are similar, the region is considered as "skin region" and used as seed for a region growing algorithm applied on neighbor non-skin regions. Finally, the explicit skin detection algorithm in Fig. 1 is applied to each pixel of detected skin regions to discard False Positive (FP) skin regions when the percentage of skin pixels in a region is above an experimental threshold. The global proposed colour based skin detection method is outlined by the algorithm pseudo code shown in Fig. 1. Some important remarks on this algorithm are the following ones.

- To recognize the skin pixels in images, we performed a training stage on the system. For this task, we obtained different skins histograms using a set of 2,314 images where the skin was manually

segmented (i.e. only skin pixels were considered). A histogram was created for each of the three channels in each considered color space (RGB, HSV and YCbCr, respectively), and its number of histogram bins was set to 10.

- The Battacharyya distance (Kailath, 1967) was used to compare the three histograms in a given color space of a test region with the corresponding ones of training skin regions histograms to decide if a region can be considered or not as skin region. This distance measures the similarity of two discrete probability distributions. Given the discrete probability distributions obtained from the corresponding histograms vectors, p and q respectively, over the same domain X, the Battachariyya coefficient BC is defined as:

Procedure ColorSkinDetection (imageIn, colorSpace, trainedSkinHistograms);
// Produces imageOUt as a binary image where skin pixels are set to 1 and non-skin pixels are set to 0
begin
if (coloSpace is 'proposed') then
Compute imageOut from imageIn using explicit skin detection directly applied to pixels
else // similar processing for 'HSV' and 'YCbCr' color spaces
Retain luminance information from imageIn;
Create an image of regions using watershed algorithm;
for each "watershed region" do
Compute histograms for the three channels in considered color space;
Compare histograms with those of trained skin region histograms using Battacharya distance;
if (value≥threshold) then Set regions as :seed skin region" and use it for region growing method
end for;
While (set of "seed skin regions: is not empty) do
Find "new skin regions" from seeds using region growing and Battachariyya distance;
Apply explicit RGB skin detection on the pixels of :skn regions" to filter "true skin regions";
Compose binary skin image imageOut by joining the set of "true skin regions"
end if
end
Algorithm 1: Pseudo code for the global colour based skin detection method

$$BC(p,q) = \sum_{x \in X} \sqrt{p(x)}\, q(x) \qquad (2)$$

where this coefficient represents is a value between 0 and 1, and the value BC=1 means the highest degree of similarity between both histograms.

Texture-based skin segmentation:

Many texture classification schemes have been used for grey level images. Texture image segmentation is common in analysis of medical images, remote sensing scene interpretation, industrial quality control inspection, document segmentation, image recovery in databases, visual recognition systems, etc. In this paper, we use a segmentation method that considers all RGB bands or other colours spaces combinations. It also permits to difference among different colour and texture combinations in the same image. It is based on the Spectral Variation Coefficient (Nunes and Conci, 2007) to evaluate region features (it can be used for very small to very large regions) and it permits to obtain correct real-time texture boundaries. It also allows distinguishing among different textures with few changes on the same type of patterns. The positional relation among the pixels on the texel (or texture element) are considered. The channels of the colour information for each pixel are combined in a new way by considering their mean and standard deviation. This scheme is computationally very efficient and it is suitable for real-time applications that combine colour and texture. It can be used for all type of texture because the texture rules of what will be identified are completely given by the used seed and are adapted to each situation. Additionally the k-means clustering technique is used to segment the regions according the SVC value for each texel band.

The first step in the calculation of the SVC for each texel is combining the information of the three original image color channels. The texel size is defined by the user or by the application. In our implementation it must have square shape, with M×M pixels, ranging from M = 3 to 21 and using odd M values (that is 3×3, 5×5,. . . , 21×21). To show how the channel combination is performed, let us use a numerical example. Consider the 7×7 texel on Fig. 2.a, represented by their intensity values for each pixel in channels R, G and B (see Figs. 2.b, 2.c and 2.d, respectively). To achieve a better characterization of the texture variations in the texel, considering also the channel order, the value of the pixel intensity of each channel (R, G or B) is substituted by a new value considering the others two channels, as shown in Fig. 3, (i.e. for the first position of the matrix). Considering the data of Fig. 2.b, the value 175 of the intensity of the first pixel in the channel R, will be changed by the result of a computation (illustrated by Fig. 3) which considers itself and the intensities of the other G and B channels (168 and 143, respectively). The new computed value will be 192,040. The same procedure will be carried out for all pixels of the input image by substituting the original pixel intensity for its new computed blended channel value. This procedure was adopted, aiming distinction of the different combinations and order of each RGB channel in the texture on analysis. The second step in the calculation of the SVC is to determine the average and the standard deviation values for each class of distances considering the used metric in the texel on analysis using the blended values. In this example of SVC computation, we are using the D4 metric, also known as Manhattan or city block distance (Sonka *et al*., 1999), to classify each pixel in the texel based on

its distance to the central position. However, any other metric can be used in the implementation of the SVC procedure. Letting q(s, t) and p(x,y) be pixels on the (s, t) and (x,y) positions respectively, then D4(p,q) is defined as:

Table 5: Sample RGB intensities of a blended Channel.

	R	G	B
C=original value	175	155	140
a	168	143	170
b	152	175	150
$x = \sqrt{a^2 + (b+1)^2}$	221,269	226,771	210,282
$y = arc\ tg(a/(b+1))$	0,802	0,682	0,743
temp value=x *x* y	190, 472	154,729	195,346
c	154,729	195,316	190,772
d	195,316	190,735	154,749
$x = \sqrt{c^2 + (d+1)^2}$	272,318	200,076	242,876
$y = arc\ tg(c/(d+1))$	0,720	0,811	0,630
new value=x *x* y	142,034	168,494	122,890

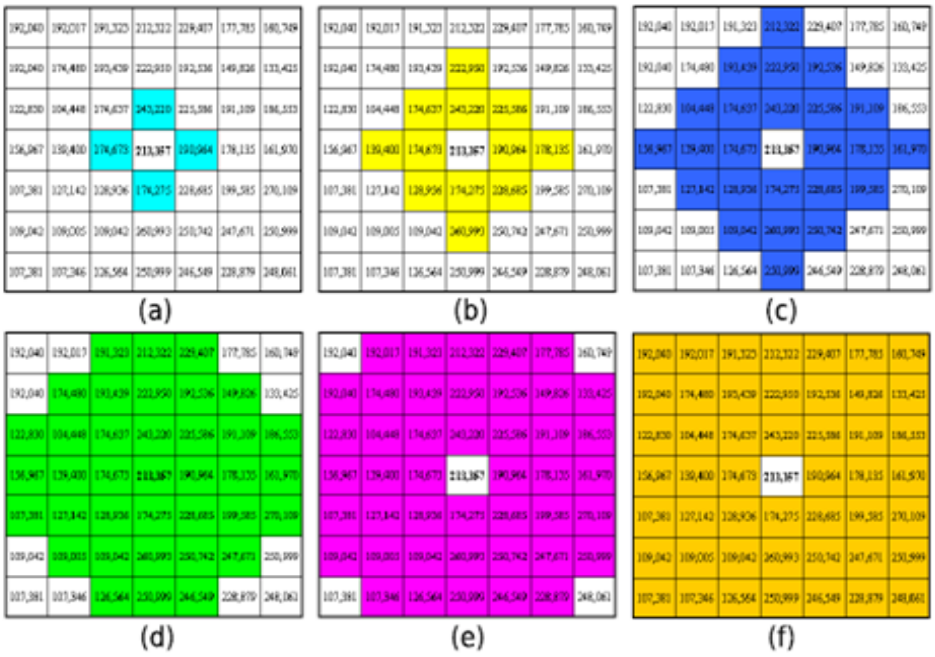

Fig 5: Six of pixels corresponding to the D4 metric distance classes on a 7x7 texel on alalysis a a) D4≤1, b) D4≤2, c)D4≤3, d)D4≤4, e) D4≤5 and f) ≤ 6D4

$$D_4(p,q) = |x-s| + |y-t| \quad (3)$$

To exemplify the calculation, consider the 6 images in Fig. 4 that illustrates the levels of intensity of one of the 3 channels after blending (R for instance) for a texel of 7×7 pixels, where each classes at different D4 distance are represented in different colour (here represented values of distance from 1 to 6). The number of D4 distance classes under consideration is, of course, related to the texel size. Finally, the SVC combines information from the space position of the pixels in the texture element (using the Fig. 4 distance classes) for each channel blended values through the mean md and the standard deviation sd inside each class of distances, thus obtaining:

$$SVD = arctg\left(\frac{md}{sd+1}\right) x\sqrt{md^2 + (sd+1)^2} \quad (4)$$

By continuing with this example and using the Figure 4 values, the SVC for each distance class associated with the R channel is computed and showed in Table 1. The value of SVC for the Red channel SVCR, corresponding to the example pixel, is computed using the values of Table 1 and eq. 3, and SVCR=393,575. The SVC of the texel is also computed for the others G and B blended channels (in the same way as shown in Fig 3 for the Red channel). This procedure can be adapted for other types of multichannel (or multiband) images. The value of the SVC in each channel of the color space defines a coordinate in the Euclidean space for the considered texel, characterizing a point in the three-dimensional space. Then, the samples of the training set are grouped by means of k-means clustering algorithm. The representative element of each cluster is its centroid, which has an average value for the

SVC considered in each canal, relative to all the samples of cluster. From an initial estimation of the coordinates of the centroids, the algorithm computes the distance of each sample of the set of training skin centroids. This way, a region is considered as "skin region" and used as seed for a region growing algorithm applied on neighbour nonskin regions if it is close to trained skin centroids. Finally, the explicit skin detection algorithm of equation 1 is applied to each pixel of detected skin regions to discard False Positive (FP) skin regions when the percentage of skin pixels in a region is above an experimental threshold. The proposed SVC-based algorithm for skin detection in the RGB color space for each texture region texelIn is outlined by the pseudo code shown in Fig 5.

Table 6: SVC computation for each distance class by considering the values of Figure 4.

Distance class	md	sd+1	SVC
1	195,783	29,203	281,627
2	195,205	40,312	272,505
3	187,198	44,971	257,026
4	184,846	49,282	250,654
5	182,863	49,760	247,336
6	182,380	49,973	246,467

Procedure SVCSkinDetection (textlIn);
//textlIn is a sample texture region where each pixel is represented by its Red, Green and Blue components
begin
for each pixel and each channel of textLIn do
Compute blending_texel value using textlIn; //as in Table 1
Compute each distance class based on each pixel position in blending_texel; //using equation(3)
for each channel of blending_texel do
for each distance class of blending-texl do
Compute mean md and the standard seviation sd values;
Compute SVC of the distance class; // using equation (4)
end for;
compute SVC of the color channel; // as in Table 2
end for;
return (SVC_R,SVC_o,SVC_B) for each channel in RGB space for region texlIN
end
Algoritm 2: Pseudo code for the SVC-based skin detection method for each texture region texln.

Table 7: Some Properties of the test images.

Image	Size (# pixels)	% skin pixels	% non-skin pixels
Ram	840,270	58.31	41.69
Sankar	607,200	35.12	64.38
Isebella	235,050	4.64	96.36
Christina	465,300	17.24	83.76

Table 8: Results for the HSV skin detection colour-based algorithm (where parameter values are [thRegion, thNeighbour, th RGB]=[0.4,0.1,0.5])

Image	Ram	Sankar	Isebella	Christina
%TP	20.01	58.82	3.53	7.54
%TN	79.45	48.18	93.10	91.75
%FP	0.13	0.80	0.31	1.92
%FN	0.11	0.31	3.15	2.32
%Suc	94.08	96.99	96.32	93.50
%Err	0.92	1.81	2.31	6.54

Table 9: Results for the skin detection SVC texture-based algorithm (the number of classes in the application of the k-means algorithm varies between 5 and 10 in the experiments)

Image	Ram	Sankar	Isebella	Christina
%TP	4.53	11.42	5.96	8.64
%TN	91.15	88.58	94.62	87.40
%FP	0.90	1.04	2.69	1.40
%FN	0.15	0.93	0.54	2.61
%Succ	97.94	98.63	96.50	95.03
%Err	2.46	1.07	3.20	3.97

Parameters Used:

i) Wrinkle Density:

The density of wrinkles in area *A* is defined as $D(1, A) = |Wa| / |Pa|$ where $|Wa|$ is the number of wrinkle pixels in area *A* and $|Pa|$ is the number of pixels in *A*.

ii) Wrinkle Depth:

The depth of wrinkles in area *A* is defined as $D(2, A) = (g\ x,)/\alpha|Wa|$ where $M\ (\ g\ (x, y)\ )$ is the canny edge magnitude of wrinkle pixel with coordinates (x, y) in *WA* and $\alpha = 255$.

iii) Average Skin Variance:

The average skin variance in area *A* is defined as $D(3, A) = (g\ x,)/\alpha \left| Pa \right|$ where $M(g(x, y))$ is the canny edge magnitude of pixels with coordinates (x,y) in P*A* and α=255. The above three wrinkle features are extracted in each of three areas.

Procedure HybSkinDetection (textlIn);
begin
for each pixel and each channel of textIn do
Compute blending_texel value using textlIn;
Compute each distance, class based on each pixel position in blending_texel;
for each channel of blending_texel do
detect edges ;
Perform HistEqual on Sat_Image;
for each edge_region do
Perform skin_detection
for each wrinkle region do
for each distance class of blending-texl do
Compute mean md and the standard seviation sd values;
Compute WrinkleDensity ds, WrinkleDepth dp and the Avg.skinVariation dv values;
Compute Hybrid_thresholds:
Compute HybSD of each class;
end for;
end for;
compute HybSD of the color channel;
end for;
end for;
end for;
return HybSD for each channel in color space for region texlIN
end

Algorithm 3: Pseudo code for Wrinkles detection

Table 10: Results for Forehead Skin Wrinkles.

Subject_Image No	Density	Depth	Skin Variance
Baby_1	0.0153	0.0285	0.0045
Baby_2	0.0312	0.0521	0.00345
Baby_3	0.044	0.0565	0.00111
Baby_4	0.0244	0.0424	0.00107
Baby_5	0.194	0.0385	0.00547
Middle age_1	0.1222	0.0468	0.00265
Middle age_2	0.1459	0.0489	0.00866
Middle age_3	0.1067	0.0344	0.0145
Middle age_4	0.1567	0.1546	0.0067
Middle age_5	0.2659	0.4590	0.0239
Seniors_1	0.25778	0.1245	0.03478
Seniors_2	0.3265	0.1569	0.06748
Seniors_3	0.3859	0.1686	0.06556
Seniors_4	0.2887	0.1768	0.07894
Seniors_5	0.7543	0.1640	0.09086

A large database of 500 facial images is taken (100 for each category) and the following steps are repeated: This paper presented and compared both a color based algorithm (using RGB, HSV and YCbCr representation spaces) and a texture-based algorithm (using the Spectral Variation Coefficient) for skin detection on color images. Although most work on skin detection is based on modelling the skin on different color spaces, we have explored the use of texture as a descriptor for the extraction of skin pixels in images. The accuracy provided by each segmentation feature based algorithm (color versus texture) is shown under different hand-segmented images. The skin detection, texture-based approach reduces in average a 13.6% the misclassified skin pixels with respect to the colour-based approach for the considered test images. A necessary future work is to validate the proposed algorithms using a standard skin database like the ECU dataset (Phung *et al*., 2005). This will permit to compare our recognition results with those presented by other authors for the same test images. Another improvement will consist in adapting our algorithms to detect skin in African or Asian people (not only white Caucasian).

RESULTS AND DISCUSSION

(A) Live Ratings:

The first test of the Wrinkle Assessment Scale was made by 15 observers (15 plastic surgeons, 15 aesthetic surgeons, and 15 dermatologists) who were asked to judge the depth of 300 mimetic wrinkles on the faces of 50 faces. Using the reference photographs depicting the Wrinkle Assessment Scale, 1000 individual ratings of wrinkle depth were made on the faces of these 50 faces (Table IV). Inter-observer variation occurred in 90 of 1100 wrinkles; 97.5 percent of the wrinkles got the same ratings (Table IV). The variations in the ratings of three plastic surgeons, 5 aesthetic surgeons, and three dermatologists showed no significant differences: 2.3 percent, 5.5 percent, and 6.2 percent of the wrinkles were rated differently from the majority of the observers.

(B) Photographic Ratings:

The next test of the wrinkle scale was performed on 250 different wrinkles by 20 independent observers (10 plastic surgeons, four lay persons). The wrinkles were marked with an arrow at their deepest point. With the aid of the photographic Wrinkle

Assessment Scale (Figs. 4 and 8 through 10), the eight observers were asked to score the depth of each of the 250 wrinkles. There was an 89.4 percent agreement among the eight observers in their classification of wrinkle depth using the Wrinkle Assessment Scale. The Wrinkle Assessment Scale was an easy, consistent, and reliable tool for the assessment of deep facial wrinkles. The scale correlated well with an objective profilometry measurement of the wrinkle depth. The most accurate description of the photographed lines and creases in our wrinkle scale is probably furrows, not folds or wrinkles. Wrinkles occur with relaxation of the skin caused by receding papillae and degeneration of elastic and collagen fibers at the dermal-epidermal junction. This degeneration starts as early as age 30 and increases with time, regardless of care and protection. The thickness of the living dermis can be determined by either ultrasound26, 27 or xero-radiographic technique. Skin thickness increases linearly up to the age of 20 years and decreases linearly with age subsequently. Depending on race, genetics, and location of measurement, the thickness of the dermis will vary.

Conclusion:

In the current era of internet advancement in skin detection methods is needed in multiple disciplines like tracking down a vehicle in an image, facial recognition, authentication purposes such as debit/credit cards, passports, voter identification cards etc. In this research, some of the application areas are highlighted and techniques of color based wrinkles in skin detection are also presented. A good classifier plays a vital role to differentiate skin and non-skin pixels in a variety of skin images with different skin types. A lot of work is done on all skin types, but experimental shortcoming is observed with sub-continental skin type detection. The future work of this research, involves the best combination of features that will help in liberalizing the values which will automatically improve the efficiency. Moreover, the issues of computational cost and memory requirements are also extremely important to be taken into account, while implemented for real-time applications.

REFERENCES

Chang, Chuan-Yu, 2010. "Automatic facial skin defect detection system."*Broadband, Wireless Computing, Communication and Applications (BWCCA), 2010 International Conference on*. IEEE.

Eisenbeiss, C., J. Welzel, W. Eichler and K. Klotz, 2001. Influence of body water distribution on skin thickness: Measurements using high-frequency ultrasound. *Br. J. Dermatol*, 144: 947.

Fitzpatrick, R.E., M.P. Goldman, N.M. Satur and W.D. Tope, 1996. Pulsed carbon dioxide laser resurfacing of photo-aged facial skin. *Arch. Dermatol*, 132: 395.

Glogau, R.G., 1996. Aesthetic and anatomic analysis of the aging skin. *Semin. Cutan. Med. Surg*, 15: 134.

Gormley, D.E. and M.S. Wortzman, 1988. Objective evaluation of methods used to treat cutaneous wrinkles. *Clin. Dermatol*, 6: 15.

Grove, G.L., M.J. Grove and J.J. Leyden, 1989. Optical profilometry: An objective method for quantification of facial wrinkles. *J. Am. Acad. Dermatol*, 21: 631.

Grover, R., A.O. Grobbelaar, B.D.G. Morgan and D.T. Gault, 1998. A quantitative method for the assessment of facial rejuvenation: A prospective study investigating the carbon dioxide laser. *Br. J. Plast. Surg.*, 51: 8.

Hamilton, D.A., 1998. classification of the aging face and its relationship to remedies. *J. Clin. Dermatol.* Summer 35.

Kligman, A.M., P. Zheng and R.M. Lavker, 1985. The anatomy and pathogenesis of wrinkles. *Br. J. Dermatol.*, 113: 37.

Lask, G., G. Keller, N. Lowe and D. Gormley, 1995. Laser skin resurfacing with the SilkTouch flashscanner for facial rhytides. *Dermatol. Surg.*, 21: 1021.

Marks, R., 1990. Method for the assessment of the effects of topical retinoic acid in photo-ageing and actinic keratoses. *J. Int. Med. Res.*, 18(3): 29C.

Muthukumar Subramanyam, Krishnan Nallaperumal, Ravi Subban, Pasupathi Perumalsamy, Shashikala Durairaj, S. Selva Kumar and S. Gayathri Devi, 2014. "Hybrid Shadow Restitution Technique for Shadow-Free Scene Reconstruction." In *Advances in Signal Processing and Intelligent Recognition Systems*, pp: 517-530. Springer International Publishing.

Muthukumar Subramanyam, Sindhu, 2015. Detecting Wrinkless and Sagginess Of Skin From Human Face Photographs, National Conference on Engineering Applications for Developing Smart Cities, 30 March 2015, ISBN:978-84743-37-6, 01(02): 415–422.

Nallaperumal, Krishnan, 2013. "An analysis of suitable color space for visually plausible shadow-free scene reconstruction from single image." *Computational Intelligence and Computing Research (ICCIC), 2013 IEEE International Conference on*. IEEE.

Olenius, M., 1998. The first clinical study using a new biodegradable implant for the treatment of lips, wrinkles and folds. *Aesthetic Plast. Surg*, 22: 97.

Rohr, M. and K. Schrader, 1998. Fast optical in vivo topometry of human skin (FOITS): Vergleichende Untersuchungen zur Laserprofilometrie. *SOFW J.*, 124: 52.

Stegman, S.J., 1987. Current techniques for soft tissue augmentation. *Video J. Dermatol*, 2: 1.

Tan, C.Y., B. Statham, R. Marks and P.A. Payne, 1982. Skin thickness measurement by pulsed ultrasound: Its reproducibility, validation and variability. *Br. J. Dermatol,* 106: 657.

Tieu, Kinh and G. Erik Miller, 2002. "Unsupervised color constancy." *Advances in Neural Information Processing Systems*.